



Contents lists available at ScienceDirect

Field Crops Research

journal homepage: [www.elsevier.com/locate/fcr](http://www.elsevier.com/locate/fcr)



## Impact of contrasted maize root traits at flowering on water stress tolerance – A simulation study

Daniel Leitner<sup>a,1</sup>, Félicien Meunier<sup>b,1</sup>,  
Gernot Bodner<sup>c</sup>, Mathieu Javaux<sup>b,d,\*</sup>, Andrea Schnepf<sup>d</sup>

<sup>a</sup> Computational Science Center, University of Vienna, Austria

<sup>b</sup> Earth and Life Institute, Environmental Sciences, Université catholique de Louvain, Louvain-la-Neuve, Belgium

<sup>c</sup> Division of Agronomy, BOKU-University of Natural Resources and Life Sciences, Vienna, Austria

<sup>d</sup> Forschungszentrum Jülich GmbH, Agrosphere (IBG-3), Jülich, Germany

### ARTICLE INFO

#### Article history:

Received 14 February 2014

Received in revised form 8 May 2014

Accepted 11 May 2014

Available online xxx

### ABSTRACT

Water stress is among the dominant yield limiting factors in global crop production. Better drought resistance is therefore a key challenge for breeding and crop management. Avoidance of water stress by effective root water uptake is considered a promising approach to yield stability in water limiting environments. Water uptake efficiency is the result of multiple plant root traits that dynamically interact with site hydrology. Root models are therefore an essential tool to identify key root traits for water efficient crops in a certain target cropping environment.

© 2014 The Authors. Published by Elsevier B.V. All rights reserved.

We present a novel combination of a dynamic root architecture model (RootBox) with a functional model of root xylem hydraulic properties and soil water flow (R-SWMS). This model integrates structural and functional root traits to simulate water uptake under variable hydrological conditions. Application of the model is exemplified for three different maize root phenotypes. We evaluate the role of root architectural and functional traits to deal with water stress at the flowering stage under two contrasted hydrological conditions (deep water storage vs. moist upper profile layer in silt loam) for a 7-day period. The phenotypes include a reference phenotype (P1), one phenotype with steeper main roots (P2), and one with steep main roots and with longer lateral roots (P3). We showed that generally those phenotypes whose root axes allocation matched with available water distribution were able to transpire more. This synchronization is a result of root architecture (structural root traits). The temporal dynamics of water depletion on the contrary were essentially determined by root hydraulic properties. We showed that lower equivalent root conductance is essentially related to a water saving behaviour of the plant, while high root conductance contributes to a water spending type with high initial transpiration that decreases quickly over time. We also showed the dramatic importance of root hydraulic property

distribution, and their relation to root order and root age, in determining equivalent root conductance and water uptake behaviour. In our simulations, increasing the radial conductivity of lateral roots by a factor 10 had more impact in the total transpiration than having different root architecture traits. It emphasizes the importance to consider not only architectural traits but also hydraulic properties in defining ideotypes and to use quantitative methods to build and test them.

Our results confirmed that functional-structural root models are appropriate to better understand the role of roots in whole plant adaptation to different drought scenarios and their contribution to distinct drought response types. The newly developed model contains all basic components to further refine complex root processes such as architectural plasticity, dynamic root conductance (xylem vulnerability, composite radial transport) and root exudation. These results could feed into cropping system models to see the effect of these processes on crop yield.

### 1. Introduction

Crop production must double by 2050 to keep pace with global population growth (Passioura, 1977; OECD/FAO, 2012). Extension of cultivated land and further management intensification is limited by growing environmental concerns and increasing costs of production factors. New ways to food security therefore require a more efficient resource use (Rockström et al., 2007; Raza et al., 2012), particularly in water-limited environments that make up 45% of global land (Safriel et al., 2005). The improvement of

\* Corresponding author at: Earth and Life Institute-Environmental sciences, Croix du Sud, 2, L7.05.02, Louvain-la-Neuve, Belgium. Tel.: +3210473708.

E-mail address: [m.javaux@fz-juelich.de](mailto:m.javaux@fz-juelich.de) (M. Javaux).

<sup>1</sup> These authors contributed equally to this work.

<http://dx.doi.org/10.1016/j.fcr.2014.05.009>

0378-4290/© 2014 The Authors. Published by Elsevier B.V. All rights reserved.

cropping systems by targeting plant-soil interactions is a largely unexploited field of agricultural management (Sposito, 2013). In this context the root system is the key plant organ for more efficient use of available resources (Lynch, 2007), particularly under stress conditions (Waines and Ehdaie, 2007). Crops have increasing competitive advantage from optimized root systems in resource limited environments due to improved water and nutrient uptake efficiency (Lynch, 2007; Hinsinger et al., 2011; Smith and de Smet, 2012).

Historic advance in breeding has largely optimized the aboveground stature of crop plants as well as their radiation use (Araus et al., 2008). It is recognized that superior root water uptake can be a crucial trait explaining superior yield of drought resistant cultivars, e.g. contributing to (flag) leaf duration, optimum pollination and grain filling (e.g. Borrell et al., 2001). Within this framework, Blum (2009) points to water uptake maximization as a focus for breeding because of its general compatibility with high yield. Taking into account the existing variability in root traits in different crops (e.g. chickpea, Kashiwagi et al., 2005; rice, Kato et al., 2006; durum wheat, Nakhforoosh et al., 2014), it can be expected that improvement of root water uptake is a feasible agronomic option. Manschadi et al. (2008) demonstrated diversity of wheat seedling root architecture. Based on field evidence and simulations studies using APSIM, they suggested that selection for growth angle and number of seminal roots may help identify genotypes with a root system that is better adapted to drought conditions. Using a model to explain historic yield trends in US maize, Hammer et al. (2009) found that changes in root architecture associated with higher water uptake to be the main reason for better abiotic stress tolerance. Using APSIM-Wheat Lilley and Kirkegaard (2011) showed that in simulations across 109 years, 5 soils, 6 management options and 6 combinations of (virtual) wheat root modifications of root system traits could result in more yield gain in dryland cropping regions. The root traits that were modified were rate of downward root penetration, efficiency of water extraction from the subsoil, an APSIM parameter for the effects of root length density, soil diffusivity and root-soil contact on the rate of water extraction. For systematic crop improvement it is therefore imperative to understand which root architecture would best contribute to maximize water acquisition under the prevalent drought stress conditions. Thus, different authors have discussed the optimal root architecture traits needed to improve plant drought tolerance (Lobet et al., 2014). For rain-fed wheat production with high importance of stored subsoil moisture, Wasson et al. (2012) showed that maximum rooting depth and shifting of rooting density to deeper layers were most relevant root traits for yield. Vadez et al. (2008) on the other hand did not find a strong correlation between root length density distribution and water uptake for groundnut in a breeding programme for a tropical residual moisture environment. They suggested to consider root functionality via water uptake and to only subsequently characterize root morphological differences between genotypes. Some authors defined root traits of apparently broad relevance for better crop growth under drought stress, such as steep, deep and metabolically cheap roots (Lynch, 2013) or root systems with fine root dominance (Comas et al., 2013). Root plasticity itself has been proposed as a beneficial trait especially when there are trade-offs between different traits (Zhang et al., 2011; Trachsel et al., 2013).

Beyond the architecture itself, different authors have also investigated the question of ideal axial and radial conductance in roots. In simulation studies, the ratio between axial and radial conductivity proved useful for classification, since this number determines if root uptake is uniformly, or preferentially from topsoil (Doussan et al., 2006; Levin et al., 2007; Draye et al., 2010). Richards and Passioura (1989) showed that reduced axial conductance of seminal roots allows water saving

during vegetative growth and help alleviate stress during the generative stage of yield formation. Other distributions of root hydraulic properties that favour water uptake are greater axial and radial conductivities in deep roots in order to increase the uptake and transport capacity of water from deep soil layers (according to Wasson et al., 2012) and, decrease of axial conductance in order to save water for the end of the crop cycle (according to Comas et al., 2013). Draye et al. (2010) pointed out the importance of the root hydraulic architecture for root water uptake, i.e. the combination of the architecture and of the distribution of the root hydraulic properties between root segments. This implies that root contribution to drought adaptation will depend on how root hydraulic properties are connected and how these eventually affect critical water use trait (Vadez, 2014).

However, the above cited studies demonstrated that not always genotypes with apparently better rooting ability provided better water uptake and/or yield improvement. A precondition to obtain better water stress tolerance via the root system is a precise definition of the target trait(s) for a clearly defined environment. In this sense root systems do not differ from what (Tardieu (2012)) stated for abiotic stress tolerance in general – any trait can confer drought tolerance, just design the right drought scenario. In climates where crops depend on stored subsoil soil water, narrow growth angle and larger numbers of seminal roots are beneficial, in climates with regular in-season rainfall, less narrow growth angles with shallower root system provide better adaptation. Seasonal drought during (late) reproductive growth is most effectively mitigated by drought escape (early maturity; e.g. Thomson and Siddique, 1997; Francia et al., 2011) as well as water saving during the vegetative stages to improve generative water availability (Mori and Inagaki, 2012). Richards and Passioura (1989) demonstrated that reducing seminal root axial conduction conserve deep water resources for grain filling. However, the precondition for successful water saving is an effective later uptake to avoid unutilized deep water after harvest. Kirkegaard et al. (2007) and Lilley and Kirkegaard (2007) quantified the value of available soil water in the subsoil for yield (i.e. additional yield per millimetre subsoil water use) and showed that its efficiency depends on management strategies that defer water use from early in the season to late in the season so that the crop uses subsoil water during grain filling. Strategies for optimizing agricultural water management first of all depend on the site specific hydrology. Yield levels in rain-fed cropping system from Mediterranean and semi-arid tropical climates largely rely on stored soil water from off-season rainfalls (e.g. French and Schultz, 1984). In these cropping environments part of the later (generative) development stages coincide with the onset of the dry season. Thus, stress sensitive processes such as flowering and grain filling are strongly related to the use of previously stored subsoil water (Kirkegaard et al., 2007). In most crops water shortage during the reproductive stage, particularly when flowering, is most detrimental for yield (Farooq et al., 2009).

Maize is a crop growing in a wide range of target environments from temperate to tropical climates, but Heisey and Edmeades (1999) estimated that one-quarter of the global maize area is affected by drought in any given year. Tollenaar and Lee (2002) demonstrated that main yield gains in maize did not come from higher yield potential or heterosis *per se*, but mainly from better stress tolerance. It has been shown that Maize is most susceptible to stress at flowering. Shaw (1977) showed that stress in the period from about 7 days before to 15 days after anthesis reduces maize grain yield two to three times more than at other growth stages. Indeed drought stress during this period increases the period between male and female flowering, widening the anthesis-silking interval (ASI) (Campos et al., 2004). Yield under stress has been

showed to be strongly dependent to kernel number per plant, barrenness and ASI in tropical Maize (Bolanos and Edmeades, 1996). Our assumption in this simulation study is that stress occurring during this period will have a major impact on the final grain yield.

Facing this complex root trait–target environment interaction and the inherent adaptive plasticity of root systems, Draye et al. (2010) suggested to develop *in-silico* experiments to test how root traits may increase drought stress tolerance. To be able to investigate the impact of root architecture on water stress tolerance, models with root growth, soil and root water flow and water uptake modules are thus required. The most sophisticated approach is to describe water movement in soil and roots simultaneously, considering the 3-dimensional root architecture, heterogeneous water distribution in the rooting zone and water potential gradients between soil and roots (Javaux et al., 2011). Root water uptake is then driven by the water potential gradients between root surface and soil.

The objective of this study is to use a mathematical model to quantitatively compare how contrasting root systems of *Zea mays* affect root water uptake pattern and soil water dynamics. We focus on the flowering period by comparing how three types of maize root architecture (called phenotypes) with different traits will suffer from stress under contrasted water conditions in a silt loam: (a) when most of the water is located at the top of the profile (SWtop) and (b) when the water content is increased in depth (SWbot). A reference phenotype (P1) is compared with two contrasted root system architectures having the same volume (proxy of the amount of invested carbon): a second type (P2) with steeper main roots and a third one (P3) based on P2 with longer lateral roots.

## 2. Material and methods

In the following we outline the mathematical model in detail, including all parameters and units. For the numerical implementation of the model we refer to the corresponding software packages that we have used, R-SWMS (Javaux et al., 2008) and RootBox (Leitner et al., 2010a).

### 2.1. Root architecture modelling

For each root, we consider three zones: the basal zone  $l_b$  at the base of the root, the branching zone, and the apical zone  $l_a$  at the end of the root (Fig. 1). After the basal and apical zones have developed their lengths stay constant during root growth, while the branching zone develops. New lateral roots are only created within the branching zone with the inter-spaces  $l_n$ .

Following Pagès et al. (1989) the root length  $\lambda$ , is dependent of the root age  $\tau$  by

$$\lambda(\tau) = k \left( 1 - \exp\left(-\frac{r}{k}\tau\right) \right), \quad (1)$$

where  $k$  is the maximal root length, and  $r$  is the initial growth speed. The maximal root length is calculated for each individual root by

$$k = l_b + l_a + l_n \cdot (nob - 1), \quad (2)$$

where  $nob$  is the maximal number of lateral branches. New lateral roots are initiated with an insertion angle  $\gamma$  which describes the angle between the parent root and the initial direction of the new lateral root. Each root has a constant radius  $a$ .

Therefore, we describe each root type in a specific soil by seven parameters:  $l_a$  [L],  $l_b$  [L],  $l_n$  [L],  $nob$  [1],  $r$  [LT<sup>-1</sup>],  $\gamma$  [1] and  $a$  [L]. To add randomness to this deterministic approach each parameter is given by its mean value and its standard deviation.

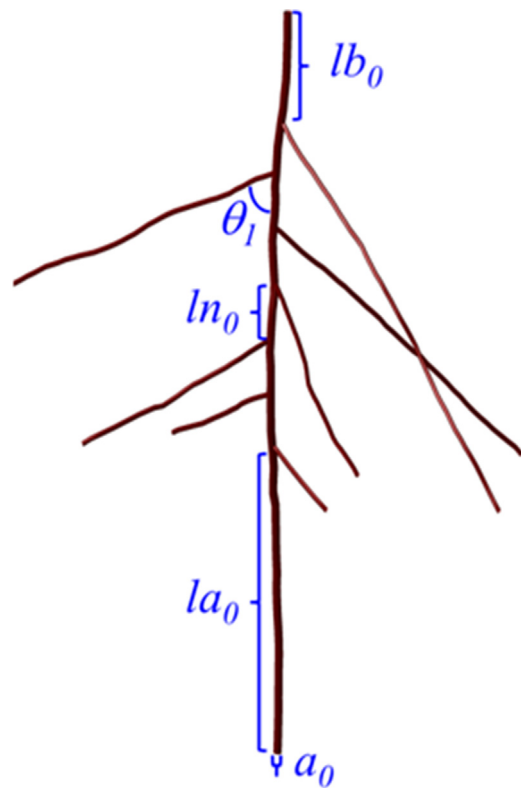


**Fig. 1.** Root growth parameters of the RootBox model. Each root order or root type is described by the length of the apical zone  $l_a$ , basal zone  $l_b$ , inter-root distance  $l_n$ , branching angle  $\theta$ , root radius  $a$ , and (not visualized) the maximal number of branches  $nob$ , and root elongation rate  $r$ .

Additionally, we describe random changes in direction during root tip elongation by randomly choosing two angles (Fig. 2). First, we choose the angle  $\alpha$ , which describes the angle between current and new root tip heading by a rotation around the local axis ( $h_y$ ). The

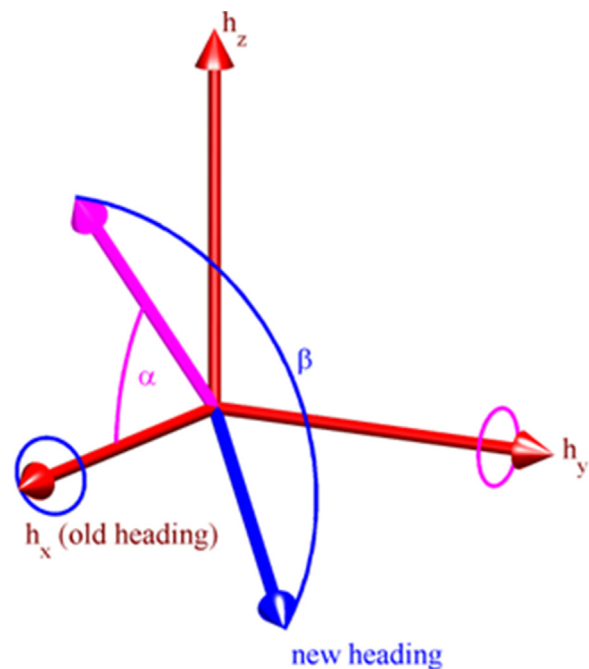


**Fig. 2.** Change of root tip heading due to two random angles  $\alpha$  and  $\beta$ .  $h_x$ ,  $h_y$  and  $h_z$  are the axes of the local coordinate system of a root segment, where  $h_x$  points into the direction of the old heading.

angle  $\alpha$  is a random number and normally distributed with a mean of 0 and a standard deviation of  $\sigma$  per root length. Thus, the expected angular change in root tip heading per unit length is  $\sigma$ . Second, we choose the radial angle  $\beta$  uniformly distributed between 0 and  $2\pi$ , which rotates the root tip heading around the local axis ( $h_x$ ).

To describe root growth towards a preferential direction (i.e. tropisms), we randomly calculate  $N$  pairs of angles ( $\alpha, \beta$ ) and then choose the most suitable pair regarding to an objective function.  $N$  is the number of trials to find optimal values for  $\alpha$  and  $\beta$ , the larger  $N$ , the more likely the root will grow in the preferred direction. The objective function is dependent on the type of tropism: for gravitropism headings into the  $z$ -direction are favoured, for exotropism headings into the initial direction, and for hydrotropism headings towards higher water content. Therefore, tropism is modelled by three parameters for each root type:  $\sigma$  [ $L^{-1}$ ],  $N$  [1], and type [1].

The main root axes of the maize plant can be implemented as crown or brace roots that start to grow after predefined times and predefined depths. The parameters for the initiation times are called  $t_{0,1}-t_{0,M}$ , and the predefined depths are given by the  $z$ -coordinates  $z_1-z_M$ , where  $M$  is the maximal number of main root axes. The root axes are initiated at a predefined angle  $\theta_0$ .

We used the L-System implementation of RootBox (Leitner et al., 2010b) to simulate the root growth model in Matlab. The dynamic growth of root systems was simulated until root systems reached a given volume. Those root systems were then used as input for simulating soil and root water flow.

## 2.2. Root water uptake and soil water flow modelling

To describe water uptake by the root system we follow the approach of Javaux et al. (2008), who combined the model of water movement in soil of Somma et al. (1998) with the model describing water flow inside a root branching structure of Doussan et al. (1998). In plants, it is common to express water potential as energy per unit volume (yielding pressure units) while it is common to describe the status of water in soils as energy per unit weight (head units). For model coupling, we chose to consistently express water potential in both systems on a volume basis.

### 2.2.1. Modelling soil water flow

Water movement in the soil is calculated with the Richards equation:

$$\frac{\partial \theta}{\partial t} = \nabla \cdot \left( \frac{K}{\rho g} (\nabla \psi_m - \rho g e_z) \right) - S, \quad (3)$$

where  $\theta := \theta(t, x)$  is the volumetric water content [ $L^3 L^{-3}$ ],  $t$  is time [T],  $x$  is the spatial coordinate [L],  $K := K(\theta)$  is the hydraulic conductivity tensor [ $L T^{-1}$ ],  $\psi_m := \psi_m(t, x)$  is the matric potential [ $M L^{-1} T^{-2}$ ],  $\rho$  is the fluid density [ $M L^{-3}$ ],  $g$  is the gravitational acceleration [ $L T^{-2}$ ],  $e_z$  is the unit vector pointing in  $z$ -direction [1], and  $S := S(t, x, \psi)$  is a volumetric sink term representing water depletion due to root water uptake per volume of soil [ $L^3 L^{-3} T^{-1}$ ]. At the top and the bottom of the domain we choose a no-flux boundary condition. At the sides, we assume periodic boundary conditions. As initial condition, we predefine a water content distribution  $\theta_0(x) := \theta(0, x)$ .

The solution for the Richards equation Eq. (3) is based on the SWMS\_3D algorithm (Šimůnek et al., 1995). The finite mesh for soil is made of cubic voxels which are automatically subdivided into 6 tetrahedral elements. A Galerkin finite element approach is applied that uses tetrahedral elements for its spatial discretization. The time component is incorporated using an implicit backward finite difference method. A solver based on a conjugate gradient method is integrated and the solution  $\psi_m(x, t)$  is obtained from a Picard iterative numerical scheme. Additional measures are taken to

improve solution efficiency in transient problems, including automatic time step adjustment.

Eq. (3) together with the initial condition and the boundary conditions allow us to simulate soil water flow, if the volumetric sink term  $S$  is known. In the following, we describe how we calculate the sink term  $S$ , taking the soil water potential, as well as the water potential distribution inside the root system into account.

### 2.2.2. Water potential distribution within the xylem network

We describe the root water pressure  $\psi_p(t, \zeta)$  in the xylem tubes, where  $\zeta$  is the arc length of the centreline of a single root segment with  $\zeta=0$  at the base of each root segment. For each  $\zeta$ , the corresponding position in Cartesian space is given by its parameterisation  $x_{root}(\zeta)$ . For a single root segment, we adapt the equation for the axial xylem water flow  $J_a$  (Javaux et al., 2008, Eq. (2b)):

$$J_a = -K_a \left( \frac{\partial \psi_p}{\partial \zeta} - \rho g \left| \frac{\partial x_{root}}{\partial \zeta} \right|_z \right), \quad (4)$$

where  $J_a := J_a(t, \zeta)$  describes the rate of axial xylem water flow [ $L^3 T^{-1}$ ],  $K_a$  is the axial root hydraulic conductance [ $M^{-1} L^5 T$ ],  $\psi_p := \psi_p(t, \zeta)$  is the pressure potential in the root xylem [ $M L^{-1} T^{-2}$ ], where  $\zeta$  is the distance from the root base [L], and  $\left| \frac{\partial x_{root}}{\partial \zeta} \right|_z$  is the absolute value of the  $z$ -component of the unit tangent vector at position  $\zeta$  [1]. The total water potential in the xylem (neglecting the osmotic potential) is  $\psi_{total} := \psi_p - \rho g$ .

Following Landsberg and Fowkes (1978) the radial water flux, which enters radially into root segments is described by

$$q_r = 2\pi a k_r (\psi_m - \psi_p), \quad (5)$$

where  $q_r := q_r(t, \zeta)$  is the rate of water flow into the root per root length [ $L^3 L^{-1} T^{-1}$ ],  $a := a(\zeta)$  is the root radius [L],  $k_r$  is the root radial hydraulic conductivity [ $M^{-1} L^2 T$ ], and  $\psi_m := \psi_m(t, x_{root}(\zeta))$  is the matric potential at the soil root interface [ $M L^{-1} T^{-2}$ ].

When no water storage is considered, the conservation of water within the root yields

$$\frac{\partial}{\partial \zeta} J_a = q_r. \quad (6)$$

This 1-dimensional partial differential equation describes the water potential in a single root section in dependence on the soil matric potential at the soil root interface.

To describe the flux distribution in a root system we stitch together multiple 1-dimensional root sections. At the nodes between the sections (i.e. the branching points) we apply Kirchhoffs law stating that the water volume flowing into the node is equal to the water volume flowing out of the node. The remaining boundaries are located at the root collar, and at the root tips. At the root collar we apply flux boundary condition under non-stressed conditions (Neumann boundary condition,  $J_{a,c} = T_{pot}$ , where  $T_{pot}$  is the potential transpiration), changing to a fixed water pressure potential when stress appears (Dirichlet boundary condition,  $\psi_{total,c} = 1.5$  MPa). At the remaining boundaries we apply a no-flux boundary condition. It results in a system of  $n_n = n_s + 1$  equations ( $n_n$  and  $n_s$  being respectively the number of root nodes and root segments), which writes in matrix notation (Doussan et al., 1998),

$$C \psi_{total} = Q, \quad (7)$$

where  $C$  (dimensions  $n_p \times n_p$ ) is called the conductance matrix which contains the root hydraulics characteristics,  $Q$  (dimensions  $n_p \times 1$ ) contains the terms related to soil and  $\psi_{total}$  (dimensions  $n_p \times 1$ ) is the unknown xylem water pressure vector (Doussan et al., 1998). Due to the large size of the system, these matrices are stored

under a sparse format to reduce memory consumption. A biconjugate gradient method is used to solve this asymmetric linear system (Press, 1996).

### 2.2.3. Implementation

The coupling between soil and the root water uptake was implemented by Javaux et al. (2008) and the software is called R-SWMS. The sink term  $S$  is calculated by summing up the radial uptake  $q_r$  of the root sections located within a soil voxel  $V$  [ $L^3$ ].

$$S(t, V) = \frac{1}{|V|} \int_V \delta_2(\chi_{\text{roots}}(x)) q_r(t, x) dx, \quad (8)$$

where  $|V|$  is the volume of  $V$  [ $L^3$ ],  $\chi_{\text{roots}}(x)$  is a characteristic function, which we define to be 0 if the Cartesian point  $x$  lies on the centreline of the root system, and else 1,  $\delta_2$  is the 2-dimensional Dirac delta function [ $L^{-2}$ ], and  $q_r(t, x)$  is the volumetric water flow per root length if  $x$  is on the root system, else 0 [ $L^3 L^{-1} T^{-1}$ ].

For coupling the water flow in both soil and root system, an implicit iterative scheme is used. First the root water flow equations given by Eq. (8) are solved given an initial estimate of the pressure head distribution in the soil. This generates a first estimate of the xylem potential  $\psi_{\text{total}}$  and water flow distribution (Eqs. (4) and (5)). A 3-dimensional sink term distribution can thus be calculated from Eq. (8), which allows the numerical solution of the Richards equation (Eq. (3)). We simultaneously solve these equations for root and soil pressure head using fix point iteration. Note that solving Eqs. (5) and (7) requires the assessment of the soil water potential in the vicinity of each root node  $\psi_m$ , defined as the average of the soil water potential of the 8 nodes of the cuboid around the root node weighted by the inverse distance between root and soil nodes.

### 2.3. Simulation scenarios

Root water uptake scenarios were run for a 7 day or a 10 day periods (for the high  $K_{rs}$  cases, see hereafter) under sinusoidal potential transpiration conditions (daily  $T_{\text{pot}} = 5.33$  mm), corresponding to typical Mediterranean climatic conditions in June–July. Simulation scenarios were built from (i) three different root system architectures (P1, P2, and P3), (ii) two distinct values for root axial conductance and radial conductivities of the root segments (indicated by the subscripts R and H), and (iii) two hydrological situations (SWtop and SWbot). This allowed studying the interactions of root system properties with the pedo-climatic environment. Given the fact that the root architecture parameters are associated with random variation (cf. > 2.1), each scenario was run in five replicates of root architecture. Each of these replicates share the same parameter sets but differ in the precise location of each root segment. Thus a total number of 60 simulations were run (3 root system architectures  $\times$  5 replicates  $\times$  2 root segment hydraulic properties  $\times$  2 soil moisture conditions).

#### 2.3.1. Root architecture

Three different types of root architectures were used and are referred to as phenotypes P1, P2 and P3 in the following text. We simulated root architectures of approximately 60 days old plants, corresponding to the flowering stage, however ensuring that root volumes were equal between phenotypes. For sake of simplicity, we modelled root systems only based on first (main roots) and secondary root orders (laterals). The first P1 is considered as a standard phenotype. The second one (P2) had steeper and deeper principal roots (as suggested by Lynch, 2013), while P3 was created based on the root system architecture of P2 but was changed to have another beneficial trait for drought resistance, i.e. fewer but

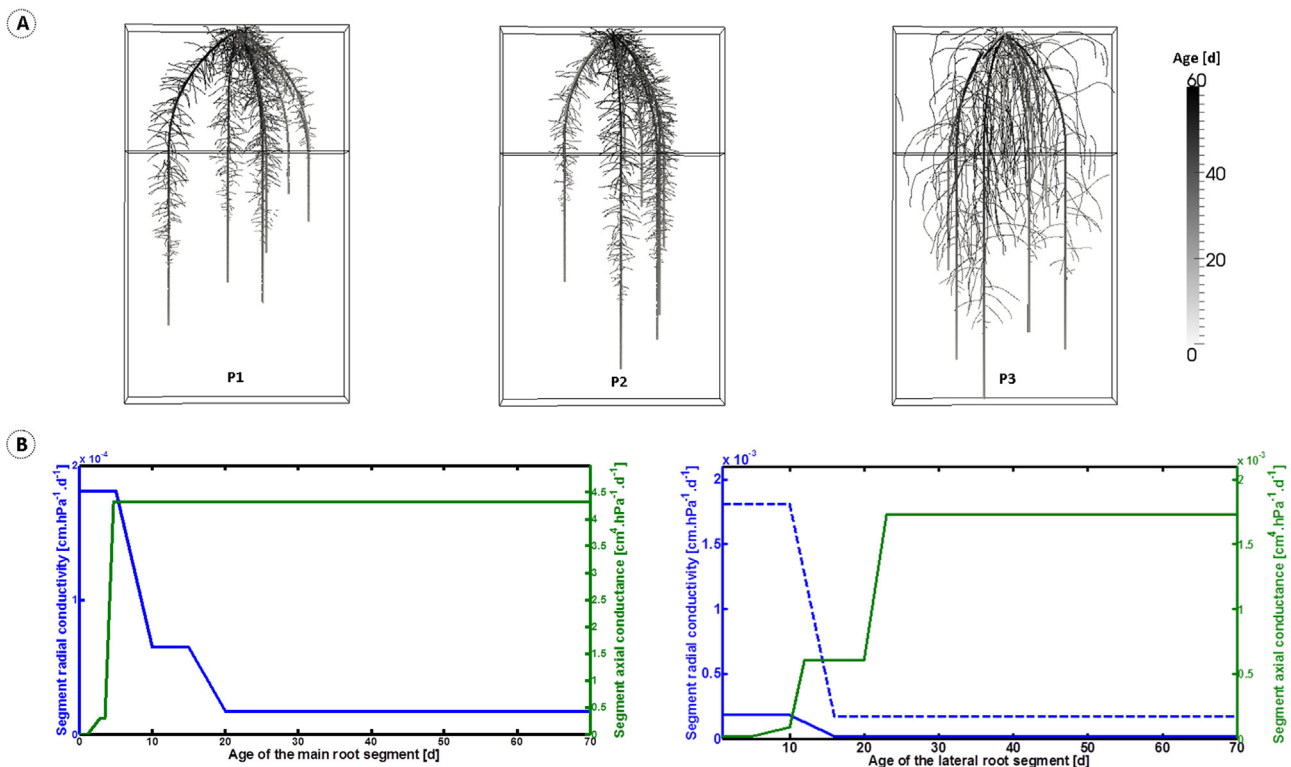


**Fig. 3.** (A) Architecture and age distribution of the root segments for a realization of each phenotype (P1, P2 and P3, respectively) and the separation line for the initial water content. (B) Age dependent root radial conductivity and axial conductance of primary (left) and lateral roots (right). In subplot B, solid and dashed lines stand for reference and increased conductivities, respectively.

**Table 1**  
Root architectural parameters for the phenotypes 1–3.

Symbol (unit)	Meaning	Parameters (primary root)	Parameters (secondary root)
$l_a$ (cm)	Length of apical zone	18.1 <sub>(P1)</sub> , 24.2 <sub>(P2)</sub> , 21.3 <sub>(P3)</sub>	10 <sub>(P1)</sub> , 10 <sub>(P2)</sub> , 100 <sub>(P3)</sub>
$l_b$ (cm)	Length of basal zone	0.5 <sub>(P1)</sub> , 0.5 <sub>(P2)</sub> , 2 <sub>(P3)</sub>	0
$l_n$ (cm)	Length of branch inter-space	0.5 <sub>(P1)</sub> , 0.5 <sub>(P2)</sub> , 2 <sub>(P3)</sub>	1.2
$nob$ (–)	Maximal number of branches	324 <sub>(P1)</sub> , 432 <sub>(P2)</sub> , 109 <sub>(P3)</sub>	0
$r$ (cm d <sup>-1</sup> )	Initial root elongation	2.94 <sub>(P1)</sub> , 3.9 <sub>(P2)</sub> , 3.55 <sub>(P3)</sub>	0.75 <sub>(P1)</sub> , 0.75 <sub>(P2)</sub> , 1.5 <sub>(P3)</sub>
$\gamma$ (rad)	Insertion angle	1.4 <sub>(P1)</sub> , 1.06 <sub>(P2)</sub> , 1.06 <sub>(P3)</sub>	1.5
$a$ (cm)	Root radius	0.13	0.05
$\sigma$ (cm <sup>-1</sup> )	Standard deviation of the root tip heading	0.1	0.1
$N$ (–)	Number of trials	2	2
Type(–)	Tropism type	geotropism	exotropism

P1: phenotype 1, P2: phenotype 2, P3: phenotype 3.

longer lateral roots at depth (Wasson et al., 2012). Fig. 3a shows one realisation of the architectural model for each phenotype P1, P2 and P3.

The 15 root systems (3 phenotypes × 5 replicates) were generated using the root growth model described in section 2.1 based on the parameters presented at Table 1. The parameterisation of P1 corresponded to the standard parameter set for maize according to Pagès et al. (1989). Two parameters of the main root axes were changed to form the parameter set describing P2: initial growth rate of the main axes was increased while their growth angle was decreased. The magnitude of these parameter changes was evaluated based on available data of the DROPS project (<http://www.dropsproject.eu/>), which screens maize genotypes for yield and root system traits. One hundred Maize genotypes were screened in aeroponics (de Dorlodot, 2005) and the extent of growth rate and insertion angle was estimated from image analysis (X. Draye, personal communication).

Table 2 summarizes the averaged root characteristics of the three phenotypes. As P2 has a higher initial growth rate of main axis, its root system is younger than that of P1 when it reaches the same volume. As P3 has longer laterals with the same root radius, the number of roots is smaller in P3 than in P2. In this way we simulate the same amount of carbon investment in different kinds of root architectures. Their effect on soil water dynamics and root water uptake during one week was simulated and in this time the root system was taken to be static.

When needed, the root length density was calculated by summing up the root length per 5 cm-deep soil compartments, considering the soil surface of 75 cm × 15 cm.

### 2.3.2. Root hydraulic properties

In order to investigate the role of the plant root hydraulic properties on root water uptake and stress onset, two cases were analysed for each phenotype: a reference scenario with hydraulic properties similar to Doussan et al. (1998) and another scenario with increased root radial conductivity. They will be referred to by

the subscripts R and H: for instance, P3<sub>H</sub> refers to phenotype 3 with higher conductivity values.

The local conductivity and conductance of the root segment for the reference scenario are taken from Doussan et al. (1998) with modifications according to Couvreur et al. (2012). Fig. 3b shows the reference (R scenario) radial conductivity and axial conductance of main and lateral roots, respectively in function to segment age. The H-scenario is based on the same values except the radial conductivity of the laterals, which is increased by a factor 10 (dotted line in Fig. 3b, right subplot) as these segments appear to be the most resistive part to water transfer. This factor ten is in the range of variations observed in experimental studies (Draye et al., 2010).

By considering a root system as a network of resistances as in an electrical circuit, the plant root equivalent conductance ( $K_{rs}$ ; cf. Table 2 for values of the three phenotypes) can be estimated using the Thevenin theorem (Couvreur et al., 2012). The actual transpiration rate [ $L^3 T^{-1}$ ] of the plant can then be defined as (Javaux et al., 2013)

$$T_{act} = K_{rs}(\psi_L - \psi_{t,eq}), \quad (9)$$

where  $\psi_L$  is the water potential at the root collar and  $\psi_{t,eq}$  is an equivalent total soil water potential, which is defined as the effective soil water potential at the soilroot-interface (Couvreur et al., 2012). The equivalent root soil water potential is the mean soil water potential of soil-root interfaces, weighted by the relative local extraction rate of the root segments in a homogeneous soil (see Eq. (17) in Couvreur et al., 2012). It is a physically sound way to define a root-sensed water potential in a heterogeneous soil. The higher  $\psi_{t,eq}$  the less energy is required to extract water from the soil. For a given amount of extracted water (represented by the cumulative transpiration), a plant with a higher (less negative)  $\psi_{t,eq}$  undergoes a less negative suction, and thus is in more favourable conditions of survival or for extracting soil water.

The evaluation of phenotype performance is done based on different indicators: (i) the equivalent soil water potential at the soil-root interface, (ii) the instantaneous stress fraction being

**Table 2**  
Averaged root statistics.

Symbol (units)	Meaning	Mean values <sup>a</sup>
$L_0$ (cm)	Total root length	6468 <sub>(P1)</sub> 6426 <sub>(P2)</sub> 7002 <sub>(P3)</sub>
$L_{comp}$ (cm)	Total root length by compartment	5104 <sub>(P1)</sub> 4606 <sub>(P2)</sub> 4348 <sub>(P3)</sub> (top <sup>b</sup> ) 1364 <sub>(P1)</sub> 1820 <sub>(P2)</sub> 2654 <sub>(P3)</sub> (bottom)
$L_{ord}$ (cm)	Total root length by order	618 <sub>(P1)</sub> 664 <sub>(P2)</sub> 759 <sub>(P3)</sub> (primary) 5850 <sub>(P1)</sub> 5762 <sub>(P2)</sub> 6243 <sub>(P3)</sub> (secondary)
$rVol$ (–)	Relative volume of the root system	1 <sub>(P1)</sub> 1.02 <sub>(P2)</sub> 1.01 <sub>(P3)</sub>
$K_{rs}$ (cm <sup>3</sup> cm <sup>-1</sup> d <sup>-1</sup> )	Equivalent conductance of the root system	0.06 <sub>(P1R)</sub> 0.062 <sub>(P2R)</sub> 0.051 <sub>(P3R)</sub> 0.17 <sub>(P1H)</sub> 0.166 <sub>(P2H)</sub> 0.091 <sub>(P3H)</sub>
Age(d)	Age at the beginning of the simulation	64 <sub>(P1)</sub> 60 <sub>(P2)</sub> 62 <sub>(P3)</sub>

<sup>a</sup> References of the scenarios are given under parentheses: P1, P2 and P3 refer respectively to phenotype 1, phenotype 2 and phenotype 3. Subscript r and h refer respectively to reference and high radial conductivity of the laterals.

<sup>b</sup> Type of initial water content distribution: top; Soil Water Top (SWtop), bottom; Soil Water Bottom (SWbot).

**Table 3**  
Parameter values for the Mualem–Van Genuchten model.

Symbol (unit)	Meaning	Parameter values
$K_{sat}$ (cm d <sup>-1</sup> )	Saturated hydraulic conductivity	10.8
$\theta_s$ (cm <sup>3</sup> cm <sup>-3</sup> )	Saturated water content	0.45
$\theta_r$ (cm <sup>3</sup> cm <sup>-3</sup> )	Residual water content	0.067
$\alpha_{vg}$ (cm <sup>-1</sup> )	Shape parameter	0.02
$n_{vg}$ (-)	Shape parameter	1.41
$\lambda_{vg}$ (-)	Shape parameter	0.5

defined as the ratio between water uptake (i.e. actual transpiration) and potential transpiration, and (iii) the cumulative water uptake as an indicator of the carbon acquired for the period.

### 2.3.3. Soil hydraulic properties

The soil was defined as a silt loam with soil hydraulic parameters from Carsel and Parrish (1988) (see Table 3). Its water retention curve, which relates the soil matric head ( $h = \frac{\psi_m}{\rho g}$ ) to the volumetric soil water content  $\theta$ , and the functional form of the hydraulic conductivity tensor  $K(h)$  are shown in Fig. 4. They were modelled using the van Genuchten–Mualem functions (Mualem, 1976; van Genuchten, 1980) using six parameters: saturated water content  $\theta_s$  [L<sup>3</sup> L<sup>-3</sup>], residual water content  $\theta_r$  [L<sup>3</sup> L<sup>-3</sup>], the saturated hydraulic conductivity  $K_{sat}$  [LT<sup>-1</sup>] and the parameters  $\alpha_{vg}$  [L<sup>-1</sup>],  $n_{vg}$  [1], and  $\lambda_{vg}$  [1], which describe the curvature of the function.

### 2.3.4. Hydrological regimes

To account for different climatic conditions in a very simple way, we consider two possible conditions for the initial water content  $\theta_0(x)$ . In the first case (called SWbot), most of the water is located at the bottom of the profile. This hydrological condition is representative for summer dry climates with high importance of subsoil water, e.g. a Mediterranean climate or an oceanic climate during a summer dry spell. The separation between the wet soil ( $\psi_{m,bot} = -100$  hPa) and the dry one ( $\psi_{m,top} = -3000$  hPa) was set at the first third of the soil depth (42 cm). In the second scenario (SWtop), the boundary is in the same location but the water content is higher close to the soil surface ( $\psi_{m,top} = -100$  hPa and  $\psi_{m,bot} = -3000$  hPa). This second case mimics a climatic situation with dominant role of regular rainfall input for plant water supply and low subsoil water reserves. Such conditions are found particularly for climates with dominant in-season rainfall during the vegetation period (e.g. semi-arid continental climates in the temperate zone), semi-arid tropical conditions before refilling of deep soil profile layers during the rainy season and for irrigation during a dry season.

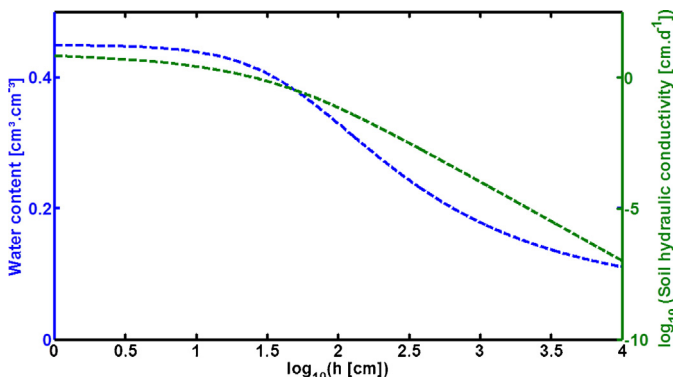


**Fig. 4.** Water retention and hydraulic conductivity curves of the soil used for the simulation.

## 3. Results

We will first present the impact of different types of root traits (phenotypes) using the reference hydraulic properties, while in the second part we will compare the impact of increased root radial conductivity. For the sake of clarity, the three phenotypes will be associated with a unique colour code in the subsequent plots: P1 will be in red, P2, in green and P3 in blue.

### 3.1. Influence of root system architecture

Fig. 5 shows the distribution of the water content for the scenario SWbot after 6.5 days for one given replicate of each phenotype. Video S1 (supplementary material) shows the evolution of the water content distribution for 7 days for the same scenario. We observe that the impact of the initial water distribution remains visible over the whole period, and that the high hydraulic pressure gradient between the two soil layers generates upward water flux. The effect of the root water uptake is also clearly visible, and we can distinguish through the water depletion pattern the main features of the root architectures of the three phenotypes. In the videos, the day–night dynamics is visible through the redistribution of the water content during night.

To investigate the difference between phenotype behaviours better, we can look at the transpiration dynamics of the three phenotypes under the two opposite hydrological regimes. In Fig. 6, the averaged transpiration of the five replicates is shown for each phenotype and for the SWbot case (Fig. 6a) and for the SWtop case (Fig. 6b). As standard deviations between replicates are small (always smaller than 3% of the mean value), they are not shown on the plots. For all phenotypes and cases, a water stress (i.e. a decrease of the actual transpiration as compared to the potential demand) is observed after the beginning of the first day of simulation and its magnitude increases with time.

If we compare both scenarios, we can see that generally these three phenotypes transpire more when the upper layer is wetter: all the phenotypes transpire more than 25 mm after 7 days for SWtop conditions (Fig. 6b), while none of them could reach 25 mm for SWbot (Fig. 6a). When we compare the change of total transpiration between SWbot and SWtop, we observe differences between phenotypes. For P3, the change of cumulative transpiration is very small (2 mm), for P2 of about 5 mm and for P1 of about 8 mm, demonstrating a different sensitivity to climatic conditions.

In the SWbot scenario (Fig. 6a), the ranking between the three phenotype transpiration rates evolves with time. While P1 and P2 have the highest transpiration rate at the beginning of the period, transpiration of P3 is highest at the end. Here P1 with a surface near root distribution undergoes a more severe stress and transpiration falls below the other phenotypes at the second day. The phenotypes with deeper root system allocation behaved similar, with the phenotype P3 having a similar behaviour between days of the whole simulation period.

In the scenario with wetter top soil layer (SWtop, Fig. 6b), it is observed that the two phenotypes P1 and P2 behave similarly while the phenotype P3 suffers from a more drastic transpiration decrease.

Fig. 7 shows the change of the equivalent soil water potential  $\psi_{t,eq}$  with increasing water extraction from soil between the beginning and the end of the period, expressing the global moisture deficit that builds up at the root–soil interface. Logically, we see that  $\psi_{t,eq}$  has a decreasing trend with time and cumulated uptake. During the night however,  $\psi_{t,eq}$  gets less negative, as the system relaxes: water potential gradients built up during day around the root segments decreases as the uptake is reduced and soil water redistribution occurs.

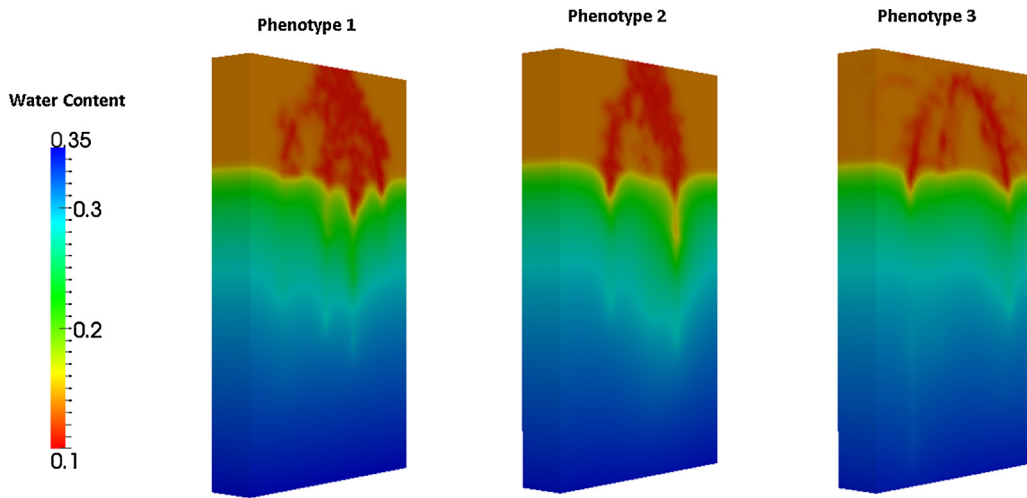


Fig. 5. 3-dimensional visualisation of soil water content as influenced by reference hydraulic architecture of the three phenotypes after 6.5 days for the SWtop scenario. See corresponding videos in supplementary material S1 and S2 for reference and increased hydraulic properties, respectively.

In the SWbot case (continuous lines), all phenotypes experience a lower soil water potential (and a lower total transpiration) than in the SWtop scenario. However, in SWbot the phenotype P3 is most efficient, as it transpires almost the same amount of water as P2 and experiences higher (less negative) soil water potential. Thus, it could be expected that P3 would be able to sustain a higher transpiration compared to P2 over a longer period of stress as it can access water more easily at depth. In the case where the water is in the upper layer (dashed lines), P1 has always a higher (less negative) total equivalent water potential than P2 and P3 for a similar given amount of cumulated transpiration. As can be expected, the deep rooted phenotype P3 (continuous blue line) not only transpires less (i.e. experiences a more severe stress) but also undergoes a lower (more negative) total equivalent water potential. However, as already observed for the transpiration

dynamics, P3 has a relatively similar behaviour between SWbot and SWtop cases.

Fig. 8 a and b show the averaged sink term profiles of the three phenotypes at two different times ( $t=0.5$  and 6.5 days) and under variable hydrological conditions. Fig. 8d shows the root length density profile of the three phenotypes: P1 has more roots at the top, P3 deeper rooting distribution and P2 an intermediate distribution. When the water is in the bottom layer (SWbot scenario, Fig. 8a), all plant phenotypes decrease their water uptake in the upper layer after 6.5 days while remaining stable in the bottom layer (Fig. 8a: dashed and continuous lines overlap in the bottom layer). Although the water content in the upper layer is low in this scenario, the three phenotypes are able to extract it at the beginning of the period, as they have a lot of roots there. The phenotype P3 has more ability to extract the soil water from

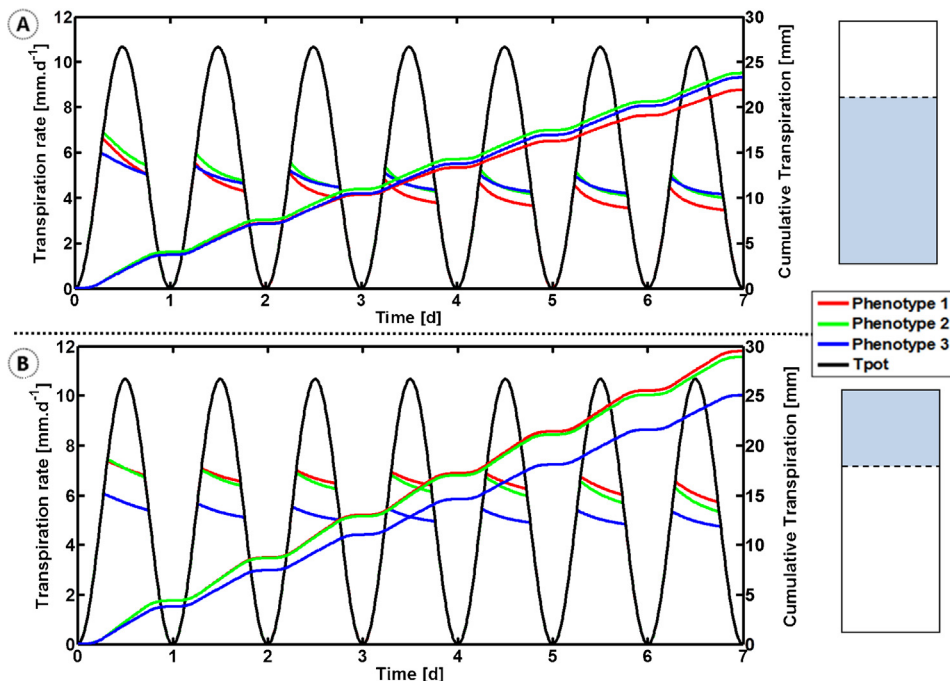
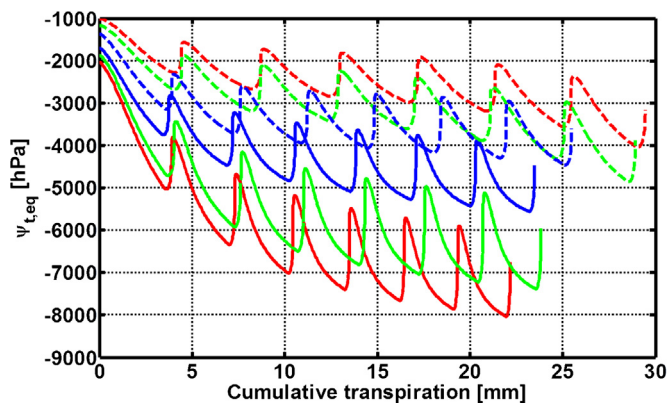


Fig. 6. Average actual and cumulative transpiration of the three phenotypes in SWbot (A) and SWtop (B) scenarios. Red: phenotype 1; green: phenotype 2 and blue: phenotype 3. The potential transpiration is represented by the black solid line. (For interpretation of the references to colour in this figure legend, the reader is referred to the web version of this article.)



**Fig. 7.** Equivalent total soil water pressure as a function of the cumulative transpiration for SWbot (solid lines) and SWtop (dashed lines). Red: P1, green: P2 and blue: P3. (For interpretation of the references to colour in this figure legend, the reader is referred to the web version of this article.)

deeper layer below 80 cm from the beginning of the period on. On the opposite, phenotype P1 extracts soil water less deep and suffers from stronger stress (see Fig. 7).

When water is located in the upper layer, P1 and P2 are able to take up more water from that horizon as compared to P3 (Fig. 8b). As P3 cannot compensate this lower uptake in the upper horizon by a much higher uptake in the drier bottom horizon, it suffers from earlier stress.

Fig. 8c shows the water changes over the whole simulation period for case SWbot (continuous lines) and SWtop (dashed lines) between phenotypes, this is not reflected in the soil water content changes. Indeed water content changes not only in function of the sink term  $S$  but also due to the water pressure distribution in the soil which generate water flow. This is particularly clear near the interface between the wet and dry zones, where water changes occur due to water and thus matric potential differences.

When we compare the sink to the root length density profiles (Fig. 8d), we hardly see any direct correspondences for any phenotypes. This is due to the fact that water is preferentially extracted where the water is available. In addition, the root length density profile only partially reflects the distribution of the root

ability to extract water. The hydraulic architecture i.e. how the root ability to extract water is distributed into the soil, combined with the water availability control the uptake (Javaux et al., 2013).

To summarize, we observed that (1) P1 which has more roots in the upper layer is very efficient in the SWtop case, but has low ability to deal with a drier upper layer; (2) P3, which has more deeper roots outperforms for SWbot; (3) P2 transpires as much as P1 for SWtop and as much as P3 for SWtop. However, its equivalent soil water potential is always more negative than the two other phenotypes.

### 3.2. Influence of root hydraulic properties

It was shown in section 3.1 that root architecture determines the extraction pattern. In this section, we investigate how distinct root hydraulic properties influence water extraction and stress onset. By increasing the radial local conductance of the laterals (H case) and comparing the performance of the 3 genotypes as compared to their initial conductance values (R case), we can assess the impact of the hydraulic properties on root water uptake.

The root equivalent conductance  $K_{rs}$  (see Eq. (8)) is a key parameter which characterizes the hydraulic architecture, i.e. the impact of the root system architecture and of the distribution of the root segment hydraulic properties. As the local hydraulic properties depend to the root order (main or lateral) and to the age of the root segments (see Table 2 and Fig. 4d), each phenotype has a different  $K_{rs}$ . Values of the mean plant equivalent conductance  $K_{rs}$  for the six cases are given in Table 2. Phenotypes P1 and P2 typically have a relatively similar  $K_{rs}$ , as they have a similar proportion of root segment age and order. We observe the following ranking:  $K_{rs}(P3_R) < K_{rs}(P1_R) < K_{rs}(P2_R) < K_{rs}(P3_H) < K_{rs}(P2_H) < K_{rs}(P1_H)$ . Multiplying the radial conductivity of the laterals by 10 increases the  $K_{rs}$  by a factor 2.8, 2.7 and 1.8 for P1, P2 and P3, respectively, as root segment age and order differ between phenotypes.

The change of water content is visualized in the supplementary material Video S2 for the higher conductance (P1<sub>H</sub>, P2<sub>H</sub> and P3<sub>H</sub>) and the SWBot scenario. As compared to P1<sub>R</sub>, P2<sub>R</sub> and P3<sub>R</sub> (see Video S1), the extraction patterns are reinforced. Table 4 shows the amount of transpiration after 7 days for the two hydrological regimes, the three phenotypes and the two  $K_{rs}$ . Higher  $K_{rs}$  always increases the amount of extracted water. Under the SWtop

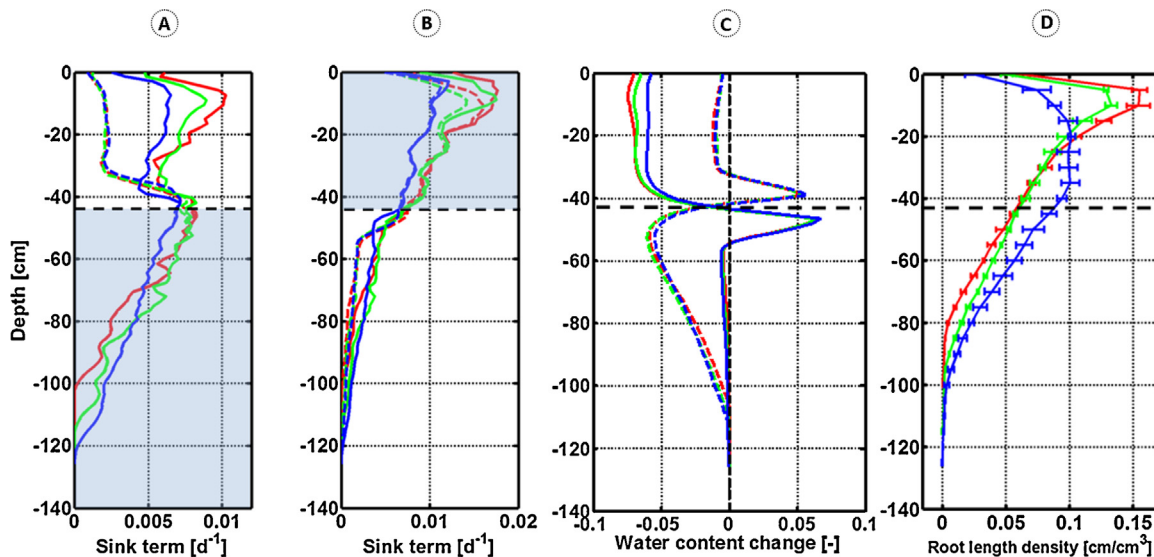


**Fig. 8.** 1-D sink term profile under scenario SWbot (A) and SWtop (B) after 0.5 (solid lines) and 6.5 (dashed lines) days and corresponding water changes (C) and root length densities (D). Red: P1, green: P2 and blue: P3. (For interpretation of the references to colour in this figure legend, the reader is referred to the web version of this article.)

**Table 4**  
Cumulative transpiration [mm] and percentage of the total potential transpiration effectively transpired after seven days for each scenario.

	P1		P2		P3	
	R	H	R	H	R	H
SWtop	29.5/79.1	37.3/100	28.9/77.5	37.3/100	25.2/67.5	36/96.5
SWbot	21.9/58.7	32.5/87.1	23.8/63.8	34.6/92.7	23.3/62.5	29.7/79.6

scenario, we do not observe any stress (100% of the  $T_{pot}$  is extracted) for P1<sub>H</sub> and P2<sub>H</sub>, while P3<sub>H</sub> suffers from a slight stress. For SWtop, the different root system architectures generate a actual transpiration difference of 12% between phenotypes. By increasing the conductance of the laterals, there is almost no impact of the root system architecture anymore. For SWBot, stress still occurs for all phenotypes with higher  $K_{rs}$ . However, differences between root architecture generate only 5–8% difference of actual transpiration while a difference in  $K_{rs}$  increases the actual transpiration by 20–30%.

In the following, we focus on the scenario with predominant subsoil water dependence SWbot, and on the two root phenotypes P2 and P3 with adapted root distribution for such hydrological conditions.

Fig. 9 compares the transpiration dynamics of P2 and P3 with reference and increased root radial conductivities for a 10 days period. When the local radial conductivity of a plant root is increased, its capacity to extract water is improved (i.e.  $K_{rs}$  increases and roots pose less resistance to water uptake and movement inside the root system), and thus transpiration is higher for a given potential difference between soil and root (see Eq. (9)). We observe that the ranking of cumulative transpiration over 10 days follows the ranking of the  $K_{rs}$  explained here before.

While the two phenotypes behave rather similar in the SWbot scenario when the reference hydraulic properties are used (denoted a P2<sub>R</sub> and P3<sub>R</sub>), there is a more distinct differentiation when considering an increased  $K_{rs}$  (denoted as P2<sub>H</sub> and P3<sub>H</sub>). Indeed, P2<sub>H</sub> is superior in transpiration compared to P3<sub>H</sub> over the 10 days of simulation. Still P2<sub>H</sub> also shows a stronger decrease in transpiration rate compared to P3<sub>H</sub>, which would result in higher stress over prolonged dry periods. Indeed, after 10 days, P3<sub>H</sub> gets a higher daily transpiration rate than P2<sub>H</sub>. In general, whatever its  $K_{rs}$ , P3 remains more stable over the simulation period, and always has a higher transpiration rate than P2 at the end of the simulation period.

Fig. 10 gives another perspective on the comparison between both phenotypes. It shows the instantaneous stress fraction

( $T_{act}/T_{pot}$ ) as a function of the fraction of the water extracted from the soil (called hereafter soil water depletion D) defined as:

$$D(t) = 100 \frac{\theta_{ini} - \theta(t)}{\theta_{ini} - \theta_r} \quad (10)$$

with  $\theta_{ini}$ ,  $\theta_r$ ,  $\theta(t)$ , the initial, residual and at time  $t$  water content of the soil, respectively. The instantaneous stress fraction reflects the reduction in transpiration and thus, the stomatal closure at a given time  $t$ . A plant with higher stress fraction keeps its stomata open so that carbon acquisition is not decreased and thus suffers less from water shortage. In Fig. 10, we observe that the water depletion is higher for phenotypes with higher root conductance  $K_{rs}$ . We also see that for a given amount of extracted water, the high  $K_{rs}$  phenotypes (P2<sub>H</sub> and P3<sub>H</sub>) experience less stress. It clearly illustrates that the water availability for plants is not only a question of soil type but also of root conductance. P2<sub>H</sub> for instance is able to extract the potential transpiration rate at the beginning of the period without reduction, due to its high  $K_{rs}$ . If we compare this with Fig. 9, we see that P2<sub>H</sub> is able to extract more water over first part of the simulation period and thus has a stronger trend to deplete available water. P3<sub>H</sub> on the contrary has a sustained water extraction over longer times. At the end of the periods P3 phenotypes have always higher cumulated water extracted with a higher water potential than P2 phenotypes, i.e. a better resistance to prolonged drought period.

This corresponds to two different strategies for the considered period: P2<sub>H</sub> takes as much water as possible at the beginning but reduces more strongly its transpiration stream, while P3<sub>H</sub> has a more conservative behaviour, keeping a constant transpiration rate with time. Note that there is no difference in the way how stress onset is represented or parameterised between scenarios. This difference is only due to a different root hydraulic architecture, i.e. P2<sub>H</sub> has a higher  $K_{rs}$  than P3<sub>H</sub> which allows more water uptake at the beginning but more stress at the end of the simulation time.

#### 4. Discussion

Agriculture has to achieve a more efficient use of water to cope with future needs of food production and competition between different fresh water users (Rockström et al., 2007). This can be achieved by reducing losses via soil management change (e.g. mulch coverage) and more efficient water acquisition by improved crops (e.g. Passioura, 1977). Root architecture and functioning are key crop traits in rain-fed cropping systems where yield depends on optimum use of site-specific water availability during the growing season.

Two main challenges to breeding for efficient root systems so far are: (i) selection of an appropriate root target trait, and (ii) ensuring that this trait effectively conveys improved crop water supply. Vadez et al. (2008) demonstrated that structural knowledge of root systems alone is not sufficient to understand different water uptake capacity among chickpea cultivars. Our study clearly sustains this empirical observation: although there is a relation between the distribution of water availability and root axes allocation in the soil profile, root functionality as expressed by root equivalent conductance appeared as key variable to infer superior water uptake of a given phenotype. A main finding of our study is that root length density distribution alone is not sufficient to describe root water uptake from soil. Root systems consist of dynamic populations of roots of different types and age, with age dependent root axial conductances and radial conductivities (Draye et al., 2010). As in Doussan et al. (2006) our model is based on combining root architectural, root system hydraulic and soil hydraulic properties including the possibility of compensation and redistribution. In our study, the difference in water acquisition induced by different architectural root traits (the 3 phenotypes)

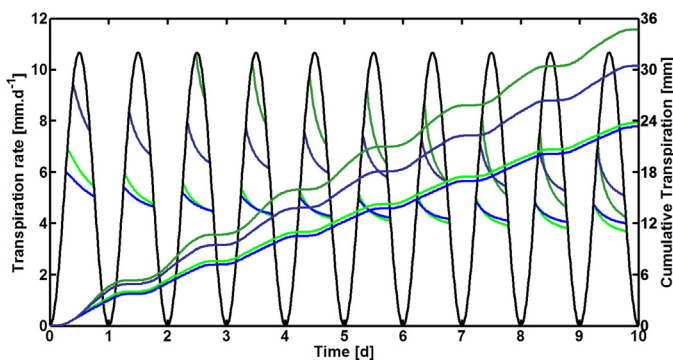


**Fig. 9.** Actual and cumulative transpiration change for P2 with reference (light green, P2<sub>R</sub>) and increased (dark green, P2<sub>H</sub>) root radial conductivity and P3 with reference (light blue, P3<sub>R</sub>) and increased (dark blue, P3<sub>H</sub>) root radial conductivity for the SWbot scenario. The black solid line is the potential transpiration. (For interpretation of the references to colour in this figure legend, the reader is referred to the web version of this article.)

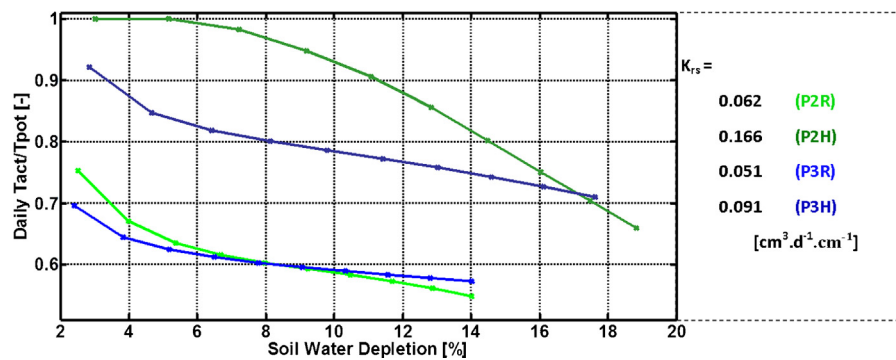


**Fig. 10.** Reduction of the actual to potential transpiration ratio for a ten days long simulation as a function of the soil water depletion in the soil (in %). Blue lines are for P3 and green lines for P2. Dark colours stand for root systems with an increased radial conductivity and light colours for reference lateral conductivities, both are for the SWtop scenario. The initial classification of the root systems is determined by the value of the root equivalent conductance (recalled on the right). (For interpretation of the references to colour in this figure legend, the reader is referred to the web version of this article.)

was much smaller than the increase induced by increasing radial hydraulic conductivity of lateral roots by a factor 10 (Table 4). This demonstrates that root architectural traits *stricto sensu* are not sufficient to explain water uptake from soil by plant roots, but root architecture and related age distribution of root segments is important for overall conductance. This is in line with the conclusions of Vadez (2014).

Within the dehydration avoidance type of drought resistance strategies, Levit (1980) distinguished between water savers and water spenders. Our study showed that root traits can confer both, water saving and water spending on a short period. The P3 root phenotype was a water saver. Concerning root system architecture (distribution) P3 had comparatively highest allocation of the sink to deeper layers and comparatively less sink strength in upper layers (Fig. 8). Whenever upper layers contributed essentially to water supply, P3 thus had lowest transpiration. However with increasing depletion P3 could sustain uptake from deeper parts of the profile over longer times (Figs. 9 and 10). The prolonged uptake from the deeper layer is related to the lower sink strength leading to a less intense depletion. The other phenotypes had a more water spending behaviour with quick initial depletion and stronger decrease of transpiration over time. For overall crop performance the importance of high short term water extraction vs. low sustained uptake depends on the drought scenario. If only intermittent dry spells have to be buffered, a water spending depletion root phenotype is more efficient as such a behaviour will keep stomata more open. In case of longer dry periods however a root phenotype conferring water saving will improve crop water supply. Here we do not consider potential competitive effects between plant water uptake and transpiration losses from upper layers. Generally water saving is only effective for stored soil moisture in deeper layers not prone to evaporation losses.

Traditionally, water uptake simulation mainly considered root distribution, with more recent architecture models giving a better insight into the 3D structure of root systems (Draye et al., 2010). More recently a focus was on integrating root functionality into architecture models. While some cropping system models like APSIM (Keating et al., 2003) used an empirical parameter for functionality, more mechanistic approaches strive to consider root hydraulic architecture as such (e.g. Sperry et al., 1998). Our results showed that differentiation between phenotypes P2 and P3 became more evident when considering root conductance (Table 4). Under a high conductance scenario, P2 showed a substantial increase in initial water uptake with values near the potential transpiration, followed by a quick decrease. Thus the water spending behaviour was accentuated. For P3 there was also an increase in the transpiration level, still the extent was less compared to P2 and this rooting phenotype maintained a more

stable transpiration level even at higher root hydraulic conductance. The stronger differentiation between P2 and P3 in the high conductance scenario was due to the age dependence of this root functional trait. As P3 contained younger root segments in deeper layers with still lower axial conductance, the bulk increase in root conductance ( $K_{rs}$  cf. Table 2) is less important. This is in line with the findings on the role of root conductance for transpiration resumed by Comas et al. (2013) who stated that generally highly conductive large diameter xylem vessels are related to high levels of (unstressed) transpiration, while lower diameter vessels induce water saving.

The differentiation between P2 and P3 at the high conductance scenario also indicates that still there was significant uptake capacity from the upper soil compartment. The substantially higher initial transpiration of P2 was mainly a result of enhanced uptake for upper layer. As revealed by the sink distribution (Fig. 8), the higher root length density in the upper compartment resulted in substantial proportion of water extracted for the upper part of the profile particularly during the first days. The sink distribution reveals that with the advance of depletion over time, upper layer extraction was increasingly source limited, while towards lower layers sink strength was limited by the lower rooting density, i.e. it was more sink limited. The sink strength in the upper compartment was further increased in the high conductance scenario, leading to an efficient and quick exploitation of extractable water resources (not shown). In the lower layers sink strength was not only limited by root distribution but further decreased in proportion to the upper layer by the lower conductance of young segments. Following Fitter's terminology (Fitter, 2002), root system architecture thus determines the overall exploration capacity of the soil profile via synchronization of water availability and depth distribution of root segments (source-sink synchronization), while root functionality (partially reflected in the root equivalent conductance) defines its capacity to exploit the available water, supporting the spending vs. saving behaviour.

In order to sustain yield under drought conditions, breeders need to blend together all knowledge on drought tolerance-related traits and their phenotypic expression (Cattivelli et al., 2008). It remains difficult to assess the overall effect of traits contributing to drought tolerance, because several traits can play roles, and these traits are likely to interact with one another and with the environment.

## 5. Conclusions

We simulated two contrasting hydraulic regimes to analyse the performance of root phenotypes with surface near root allocation (P1) vs. steeper root allocation (P2 and P3), where P2 and P3

correspond to deep and steep phenotypes with high lateral growth for P3. As expected, superiority of a given root architecture was dependent on the water regime. For the soil conditions used here, our simulations showed that a deep and steep phenotype is beneficial only in situations where crop water supply depends on subsoil moisture while surface-near allocation of roots is more preferential when crops can rely on high in-season rainfall. This corresponds to findings from vegetation ecology and ecohydrology (e.g. Schenk and Jackson, 2002; Preti et al., 2010).

Although the root systems of the three virtual phenotypes considered in this study have the same volume, they behave quite differently in terms of water uptake from soil.

In general, the same amount of carbon spent can create different root system architectures with different hydraulic properties that will affect overall water uptake behaviour.

In particular, the root length density profile is not sufficient to characterize root system water uptake efficiency. In this simulation case study we kept the overall amount of carbon spent constant and compared the effect when the carbon was spent into more or less deep and steep root system architectures. However, this results in the fact that we did not model the cheap aspect of the ideotype of Lynch (2013), which could also affect the conclusions of this study regarding root system water uptake efficiency.

Regarding the hydrological conditions, phenotype P3 that had fewer and longer laterals was better in a situation that can be found in climates with a dry summer and high importance of subsoil water: it has a more conservative behaviour on a longer term. For plants with comparable rooting depth, the overall root system conductance  $K_{rs}$  is a key parameter to explain transpiration dynamics.

The plant root systems we created were generic, although the variability of parameters was chosen in correspondence with the genotypic variations of maize root systems analysed in the DROPS project for drought tolerant yielding plants. We demonstrated how root architecture and hydraulic properties can induce different behaviour, also as a function of the environment considered, and thus one should be careful while designing an ideotype based on root architectural traits alone. Beyond the root architecture itself, the age distribution and related root hydraulic properties need to be considered. These results could feed into cropping system models to see the effect of these processes on crop yield.

## Acknowledgments

This work is a contribution of the Transregio Collaborative Research Center 32, Patterns in Soil–Vegetation–Atmosphere Systems: Monitoring, Modelling and Data Assimilation, which is funded by the German Research Association, DFG. This work has also been funded in part by the project DROPS (DROught tolerant yielding Plants: <http://www.drops-project.eu>), which received funding from the European Community's Seventh Framework Programme under the grant agreement no. FP7-244374. F. M. is supported by the Fonds National de la Recherche Scientifique (FNRS) of Belgium as a research fellow. D. L. is recipient of an APART – fellowship of the Austrian Academy of Sciences at the Computational Science Center. We acknowledge the Austrian Science Fund (FWF) through grant no. V220–N13 (A.S.).

## Appendix A. Supplementary data

Supplementary data associated with this article can be found, in the online version, at <http://dx.doi.org/10.1016/j.fcr.2014.05.009>.

## References

Araus, J.L., Slafer, G.A., Royo, C., Serret, M.D., 2008. Breeding for yield potential and stress adaptation in cereals. *Crit. Rev. Plant Sci.* 27, 377–412.

- Blum, A., 2009. Effective use of water (EUW) and not water-use efficiency (WUE) is the target of crop yield improvement under drought stress. *Field Crops Res.* 112, 119–123.
- Bolanos, J., Edmeades, G.O., 1996. The importance of the anthesis-silking interval in breeding for drought tolerance in tropical maize. *Field Crops Res.* 48, 65–80.
- Borrell, A., Hammer, G., Van Oosterom, E., 2001. Stay-green: a consequence of the balance between supply and demand for nitrogen during grain filling? *Ann. Appl. Biol.* 138, 91–95.
- Campos, H., Cooper, M., Habben, J.E., Edmeades, G.O., Schussler, J.R., 2004. Improving drought tolerance in maize: a view from industry. *Field Crops Res.* 90, 19–34.
- Carsel, R.F., Parrish, R.S., 1988. Developing joint probability distributions of soil water retention characteristics. *Water Resour. Res.* 24, 755–769.
- Cattivelli, L., Rizza, F., Badeck, F.W., Mazzucotelli, E., Mastrangelo, A.M., Francia, E., Marè, C., Tondelli, A., Stanca, A.M., 2008. Drought tolerance improvement in crop plants: an integrated view from breeding to genomics. *Field Crops Res.* 105, 1–14.
- Comas, L.H.B., SR, Von Mark, V.C., Byrne, P.F., Dierig, D.A., 2013. Root traits contributing to plant productivity under drought. *Front. Plant Sci.* 4.
- Couvreur, V., Vanderborght, J., Javaux, M., 2012. A simple three-dimensional macroscopic root water uptake model based on the hydraulic architecture approach. *Hydrol. Earth Syst. Sci.* 16, 2957–2971.
- de Dordot, S., 2005. Scaling up quantitative phenotyping of root system architecture using a combination of aeroponics and image analysis. *Aspects Appl. Biol.* 73, 41–54.
- Doussan, C., Pagès, L., Vercambre, G., 1998. Modelling of the hydraulic architecture of root systems: an integrated approach to water absorption – model description. *Ann. Bot.* 81, 213–223.
- Doussan, C., Pierret, A., Garrigues, E., Pagès, L., 2006. Water uptake by plant roots: II – modelling of water transfer in the soil root-system with explicit account of flow within the root system – comparison with experiments. *Plant Soil* 283, 99–117.
- Draye, X., Kim, Y., Lobet, G., Javaux, M., 2010. Model-assisted integration of physiological and environmental constraints affecting the dynamic and spatial patterns of root water uptake from soils. *J. Exp. Bot.* 61, 2145–2155.
- Farooq, M., Wahid, A., Lee, D.J., Ito, O., Siddique, K.H.M., 2009. Advances in drought resistance of rice. *Crit. Rev. Plant Sci.* 28, 199–217.
- Fitter, A.H., 2002. Characteristics and functions of root systems. In: Waisel, Y., Eshel, A., Kafkaf, U. (Eds.), *Plant Roots: The Hidden Half*. Marcel Dekker Inc., New York, NY, pp. 21–50.
- Francia, E., Tondelli, A., Rizza, F., Badeck, F.W., Li Destri Nicosia, O., Akar, T., Grando, S., Al-Yassin, A., Benbelkacem, A., Thomas, W.T.B., van Eeuwijk, F., Romagosa, I., Stanca, A.M., Pecchioni, N., 2011. Determinants of barley grain yield in a wide range of Mediterranean environments. *Field Crops Res.* 120, 169–178.
- French, R.J., Schultz, J.E., 1984. Water use efficiency of wheat in a Mediterranean-type environment. I. The relation between yield, water use and climate. *Aust. J. Agric. Res.* 35, 743–764.
- Hammer, G.L., Dong, Z., McLean, G., Doherty, A., Messina, C., Schussler, J., Zinselmeier, C., Paszkiewicz, S., Cooper, M., 2009. Can changes in canopy and/or root system architecture explain historical maize yield trends in the U.S. corn belt? *Crop Sci.* 49, 299–312.
- Heisey, P.W., Edmeades, G.O., 1999. *Maize Production in Drought Stressed Environments: Technical Options and Research Resource Allocation*. International Maize and Wheat Improvement Center, Mexico D.F, pp. 1–36.
- Hinsinger, P., Brauman, A., Devau, N., Gérard, F., Jourdan, C., Laclau, J.P., Le Cadre, E., Jaillard, B., Plassard, C., 2011. Acquisition of phosphorus and other poorly mobile nutrients by roots. Where do plant nutrition models fail? *Plant Soil* 348, 29–61.
- Javaux, M., Couvreur, V., Vanderborght, J., Vereecken, H., 2013. Root water uptake: from three-dimensional biophysical processes to macroscopic modeling approaches. *Vadose Zone J.* 12.
- Javaux, M., Draye, X., Doussan, C., Vanderborght, J., Vereecken, H., 2011. Root water uptake: toward 3-D functional approaches. In: Gliński, J., Horabik, J., Lipiec, J. (Eds.), *Encyclopedia of Agrophysics*. Springer, Netherlands, pp. 717–722.
- Javaux, M., Schröder, T., Vanderborght, J., Vereecken, H., 2008. Use of a three-dimensional detailed modeling approach for predicting root water uptake. *Vadose Zone J.* 7, 1079–1088.
- Kashiwagi, J., Krishnamurthy, L., Upadhyaya, H.D., Krishna, H., Chandra, S., Vadez, V., Serraj, R., 2005. Genetic variability of drought-avoidance root traits in the mini-core germplasm collection of chickpea (*Cicer arietinum* L.). *Euphytica* 146, 213–222.
- Kato, Y., Abe, J., Kamoshita, A., Yamagishi, J., 2006. Genotypic variation in root growth angle in rice (*Oryza sativa* L.) and its association with deep root development in upland fields with different water regimes. *Plant Soil* 287, 117–129.
- Keating, B.A., Carberry, P.S., Hammer, G.L., Probert, M.E., Robertson, M.J., Holzworth, D., Huth, N.I., Hargreaves, J.N.G., Meinke, H., Hochman, Z., Lean, M., Verburg, G., Snow, K., Dimes, V., Silburn, J.P., Wang, M., Brown, E., Bristow, S., Asseng, K.L., Chapman, S., Cown, M., Freebairn, R.L., Smith, D.M., C.J., 2003. An overview of APSIM, a model designed for farming systems simulation. *Eur. J. Agron.* 18, 267–288.
- Kirkegaard, J.A., Lilley, J.M., Howe, G.N., Graham, J.M., 2007. Impact of subsoil water use on wheat yield. *Aust. J. Agric. Res.* 58, 303–315.
- Landsberg, J.J., Fowkes, N.D., 1978. Water movement through plant roots. *Ann. Bot.* 42, 493–508.
- Leitner, D., Klepsch, S., Bodner, G., Schnepf, A., 2010a. A dynamic root system growth model based on L-systems. *Plant Soil* 332, 177–192.
- Leitner, D., Klepsch, S., Ptashnyk, M., Marchant, A., Kirk, G.J.D., Schnepf, A., Roose, T., 2010b. A dynamic model of nutrient uptake by root hairs. *New Phytol.* 185, 792–802.

- Levin, A., Shaviv, A., Indelman, P., 2007. Influence of root resistivity on plant water uptake mechanism, part I: numerical solution. *Transport Porous Med.* 70, 63–79.
- Levit, J., 1980. Responses of plants to environmental stresses. Water, Radiation, Salt, and Other Stresses, vol. II. Academic Press, New York.
- Lilley, J.M., Kirkegaard, J.A., 2007. Seasonal variation in the value of subsoil water to wheat: simulation studies in southern New South Wales. *Aust. J. Agric. Res.* 58, 1115–1128.
- Lilley, J.M., Kirkegaard, J.A., 2011. Benefits of increased soil exploration by wheat roots. *Field Crops Res.* 122, 118–130.
- Lobet, G., Couvreur, V., Meunier, F., Javaux, M., Draye, X., 2014. Plant water uptake in drying soils. *Plant Physiol.* 164, 1619–1627.
- Lynch, J.P., 2007. Turner review no. 14. Roots of the second green revolution. *Aust. J. Bot.* 55, 493–512.
- Lynch, J.P., 2013. Steep, cheap and deep: an ideotype to optimize water and N acquisition by maize root systems. *Ann. Bot.* 112, 347–357.
- Manschadi, A.M., Hammer, G.L., Christopher, J.T., DeVoil, P., 2008. Genotypic variation in seedling root architectural traits and implications for drought adaptation in wheat (*Triticum aestivum* L.). *Plant Soil* 303, 115–129.
- Mori, M., Inagaki, M., 2012. Root development and water-uptake under water deficit stress in drought-adaptive wheat genotypes. *Cereal Res. Commun.* 40, 44–52.
- Mualem, Y., 1976. New model for predicting the hydraulic conductivity of unsaturated porous media. *Water Resour. Res.* 12, 513–522.
- Nakhforoosh, A., Grausgruber, H., Kaul, H.-P., Bodner, G., 2014. Wheat root diversity and root functional characterization. *Plant Soil* 1–19.
- OECD/FAO, 2012. *Agricultural outlook, 2012–2021*.
- Pagès, L., Jordan, M.O., Picard, D., 1989. A simulation model of the three-dimensional architecture of the maize root system. *Plant Soil* 119, 147–154.
- Passioura, J., 1977. Grain yield, harvest index and water use of wheat. *J. Austr. Inst. Agric. Sci.* 43, 117–120.
- Press, W.H., 1996. *Numerical Recipes in Fortran 90: the Art of Parallel Scientific Computing*. Cambridge University Press, New York Volume 2 of Fortran Numerical Recipes.
- Preti, F., Dani, A., Laio, F., 2010. Root profile assessment by means of hydrological, pedological and above-ground vegetation information for bio-engineering purposes. *Ecol. Eng.* 36, 305–316.
- Raza, A., Friedel, J., Bodner, G., 2012. Improving water use efficiency for sustainable agriculture. In: Lichtfouse, E. (Ed.), *Agroecology and Strategies for Climate Change*. Springer, Netherlands, pp. 167–211.
- Richards, R.A., Passioura, J.B., 1989. A breeding program to reduce the diameter of the major xylem vessel in the seminal roots of wheat and its effect on grain yield in rain-fed environments. *Aust. J. Agric. Res.* 40, 943–950.
- Rockström, J., Lannerstad, M., Falkenmark, M., 2007. Assessing the water challenge of a new green revolution in developing countries. *Proc. Natl. Acad. Sci. U. S. A.* 104, 6253–6260.
- Safriel, U., Adeel, Z., Niemeijer, D., Puigdefabregas, J., White, R., Lal, R., Winslow, M., Ziedler, J., Prince, S., Archner, E., King, C., 2005. Dryland systems. In: Hassan, R., Scholes, R.J., Ash, N. (Eds.), *Ecosystems Human Well-Being. Findings of the Conditions Trends Working Group of the Millennium Ecosystem Assessment*, vol. 1. Island Press, Washington D.C., U.S.A., pp. 623–662.
- Schenk, H.J., Jackson, R.B., 2002. Rooting depths, lateral root spreads and below-ground/above-ground allometries of plants in water-limited ecosystems. *J. Ecol.* 90, 480–494.
- Shaw, R.H., 1977. Water use and requirements of maize—a review. *Agrometeorology of the Maize (corn) Crop*. World Met. Organization, Geneva, Switzerland pp. 119–134 Publication 480.
- Šimůnek, J., Huang, K., van Genuchten, M.T., 1995. The SWMS- 3D Code for Simulating Water Flow and Solute Transport in Three-Dimensional Variably-Saturated Media. Research Report No. 139. U. S. Salinity Laboratory, Riverside, California.
- Smith, S., de Smet, I., 2012. Root system architecture: insights from Arabidopsis and cereal crops. *Phil. Trans. Royal Soc. B: Biol. Sci.* 367, 1441–1452.
- Somma, F., Hopmans, J.W., Clausnitzer, V., 1998. Transient three-dimensional modeling of soil water and solute transport with simultaneous root growth, root water and nutrient uptake. *Plant Soil* 202, 281–293.
- Sperry, J.S., Adler, F.R., Campbell, G.S., Comstock, J.P., 1998. Limitation of plant water use by rhizosphere and xylem conductance: results from a model. *Plant Cell Environ.* 21, 347–359.
- Sposito, G., 2013. Green water and global food security. *Vadose Zone J.* 12, <https://www.soils.org/publications/vzj/articles/12/4/vzj2013.02.0041>.
- Tardieu, F., 2012. Any trait or trait-related allele can confer drought tolerance: Just design the right drought scenario. *J. Exp. Bot.* 63, 25–31.
- Thomson, B.D., Siddique, K.H.M., 1997. Grain legume species in low rainfall Mediterranean-type environments II. Canopy development, radiation interception, and dry-matter production. *Field Crops Res.* 54, 189–199.
- Tollenaar, M., Lee, E.A., 2002. Yield potential, yield stability and stress tolerance in maize. *Field Crops Res.* 75, 161–169.
- Trachsel, S., Kaeppler, S.M., Brown, K.M., Lynch, J.P., 2013. Maize root growth angles become steeper under low N conditions. *Field Crops Res.* 140, 18–31.
- Vadez, V., Rao, S., Kholova, J., Krishnamurthy, L., Kashiwagi, J., Ratnakumar, P., Sharma, K.K., Bhatnagar-Mathur, P., Basu, P.S., 2008. Root research for drought tolerance in legumes: quo vadis. *J. Food Legumes* 21, 77–85.
- Vadez, V., 2014. Root hydraulics: the forgotten side of roots in drought adaptation. *Field Crops Res.* <http://dx.doi.org/10.1016/j.fcr.2014.03.017>.
- van Genuchten, M.T., 1980. Closed-form equation for predicting hydraulic conductivity of unsaturated soils. *Soil Sci. Soc. Am. J.* 44, 892–898.
- Waines, J.G., Ehdaie, B., 2007. Domestication and crop physiology: roots of green-revolution wheat. *Ann. Bot.* 100, 991–998.
- Wasson, A.P., Richards, R.A., Chatrath, R., Misra, S.C., Prasad, S.V.S., Rebetzke, G.J., Kirkegaard, J.A., Christopher, J., Watt, M., 2012. Traits and selection strategies to improve root systems and water uptake in water-limited wheat crops. *J. Exp. Bot.* 63, 3485–3498.
- Zhang, H.W., Huang, Y., Ye, X.S., Xu, F.S., 2011. Genotypic variation in phosphorus acquisition from sparingly soluble P sources is related to root morphology and root exudates in *Brassica napus*. *Sci. China Life Sci.* 54, 1134–1142.